

Effect of primary aberrations on tight focusing of second order radially polarized beam

Maruthi M Brundavanam¹ and Rakesh Kumar Singh²

¹Department of Physics, Indian Institute of Technology Kharagpur, Kharagpur-721 302, India

²Applied and Adaptive Optics Laboratory, Department of Physics

Indian Institute of Space Science and Technology (IIST), Trivandrum, 695 547, Kerala, India

(Celebrating 25th Anniversary)

Effect of primary aberrations on tight focusing of second order radially polarized beam is investigated using vector diffraction theory. A detailed analysis on the effect of spherical aberration on the focal structure of the second order radially polarized beam is carried out and results are compared with the first order radially polarized beam. It is demonstrated that the optical cage structure of the second order beam is highly sensitive to spherical aberration in addition to the truncation parameter of the beam. Susceptibility of the optical cage structure to astigmatism and coma is also investigated. © Anita Publications. All rights reserved.

Keywords: Radially polarized beam, Tight focusing, Debye-Wolf integral, Longitudinal polarization, Optical cage structure.

1 Introduction

In recent times, a considerable amount of interest has grown in studying the three dimensional structure of the optical beams in the focal region of high numerical aperture (NA) systems. Amongst all optical beams, radially polarized laser beams generate strong longitudinal electric field at the focal point in case of tight focusing [1-9]. The applications of such tightly focused beams are found in increasing the resolution in microscopy and create evanescent Bessel beam via surface plasmons [4,10]. Also, tightly focused radially polarized beams have a great importance in optical trapping, material processing, particle acceleration and data storage to name a few [11-13]. Most of the mentioned applications use first order radially polarized, R-TEM₀₁ (R stands for radial polarization) beam [1-4]. Later, it has been found that double ring shaped second order radially polarized mode, R-TEM₁₁ [14-17] can generate a sharp focal spot of longitudinal component in comparison to R-TEM₀₁ beam. The sharp focal spot in case of R-TEM₁₁ beam is due to the destructive interference occurring between the inner and outer rings with π phase shift [18-22]. The usefulness of the sharp focal spot generated by R-TEM₁₁ beam has been demonstrated using the laser scanning confocal microscope [23].

The quality of the focused beam near the focal spot of a high NA is extremely important to widen the practical applications of radially polarized beams. In high NA systems, the shape and structure of the tightly focused beams is strongly affected by the aberrations [24-29]. In order to improve the shape and structure of the tightly focused beams, it is important to study the structure of tightly focused beams in presence of aberrations. To this end, Biss and Brown [26] investigated the effect of primary aberrations on a tightly focused first order radially polarized beam and to the best of our knowledge no such investigations seems

Corresponding author :

e-mail: bmmanoj@phy.iitkgp.ac.in (Maruthi M Brundavanam); krakeshsingh@iist.ac.in (Rakesh Kumar Singh)

to exist for second order radially polarized beams. In the present paper, we investigate the effect of primary aberrations on the tight focusing of the second order radially polarized beam. The primary aberrations include spherical aberration, astigmatism and coma. The intensity distributions near the focal point of a second order radially polarized beam in presence of spherical aberration are discussed in details for different truncation parameters. The results are compared with those of the first order radially polarized beam. It has been shown that in the absence of aberrations and for a particular value of truncation parameter an interesting optical cage like structure is observed at the focal spot. The effects of astigmatism and coma on the tight focusing of second order radially polarized beam especially on the optical cage like structure are also discussed.

2 Theoretical Explanation

The complex amplitude of higher order beam at the incident plane of a high numerical aperture (NA) focusing system (see Fig. 1) can be written as [18]:

$$C_a(\theta) = \left(\frac{\beta^2 \sin \theta}{\sin^2 \alpha} \right) \exp \left(-\frac{\beta^2 \sin^2 \theta}{\sin^2 \alpha} \right) L_p^l \left(\frac{2\beta^2 \sin^2 \theta}{\sin^2 \alpha} \right) \quad (1)$$

where θ is the focusing angle (the angle between the optical axis and the given ray) as defined in Fig 1. α is the maximum angle of convergence ($\alpha = \theta_{\max}$). The maximum convergence angle and NA of the tightly focusing system are related as $\text{NA} = n \sin(\theta_{\max}) = n \sin(\alpha)$. L_p^l is the generalized Laguerre polynomial and here l and p represent the azimuthal and radial index. In the present paper, we use $l = 2$ and $p = 0, 1$. In Eq (1), $\beta = a/\omega$ is the truncation parameter which represents the fraction of the beam inside the physical aperture with ω as a parameter for the beam size. In the present case, the entrance plane of the focusing system sketched in Fig 1 is assumed to be coincided with the waist plane of the beam and amount of the incident beam passing through the focusing system is controlled by the truncation parameter, β . In the present study, because of the dominating role of polarization in focusing the radially polarized beams with high NA systems [1-9], scalar diffraction theory does not give accurate results, so Debye-Wolf integral [30] is used to represent the field distribution in the focal region. Considering the focusing geometry shown in Fig 1 and using Debye-Wolf integral, the Cartesian components of the complex field in the focal region of a high NA focusing system is given [1,30] as:

$$E(\vec{r}, z) = \begin{bmatrix} E_x(\vec{r}, z) \\ E_y(\vec{r}, z) \\ E_z(\vec{r}, z) \end{bmatrix} = (-iA/\lambda f) \int_0^\alpha \int_0^{2\pi} \cos^{1/2} \theta C_a(\theta) e^{i\Phi} P(\theta, \phi) e^{ik\hat{s}\cdot\vec{r}} \sin \theta d\phi d\theta \quad (2)$$

In Eq (2), A is a constant, λ is wavelength, f is focal length, ϕ is azimuthal angle, $k = 2\pi/\lambda$ is wave number, \hat{S} represents the direction vector of a typical ray in focal plane, $\cos^{1/2}\theta$ represents the apodization factor for an aplanatic focusing system. Φ represents the wave aberration function that denotes the deviation of the actual wavefront from the ideal wavefront. The value of Φ in presence of primary aberrations and defocusing is defined as,

$$\Phi(\theta) = \frac{2\pi}{\lambda} \left[A_s \left(\frac{\sin \theta}{\sin \alpha} \right)^4 + A_d \left(\frac{\sin \theta}{\sin \alpha} \right)^2 + A_a \left(\frac{\sin \theta}{\sin \alpha} \right)^2 \cos^2 \phi + A_c \left(\frac{\sin \theta}{\sin \alpha} \right)^3 \cos \phi \right] \quad (3)$$

where the coefficients A_s , A_d , A_a and A_c represent the strengths of spherical aberration, defocusing, astigmatism and coma in the units of wavelength of input light.

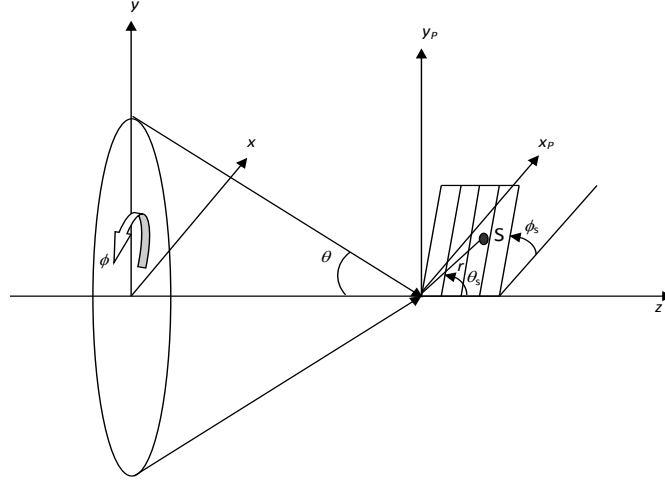


Fig 1. Geometric configuration of the problem. $S(r, \theta_s, \phi_s)$ is the observation point at the focal plane where r, θ_s, ϕ_s denote the cylindrical coordinates at the focal plane.

In Eq (2), $P(\theta, \phi)$ represents the polarization matrix that describes the coordinate system rotation that generates the electric field components after the lens. The polarization matrix at the exit plane of the focusing system $P(\theta, \phi)$ can be written as:

$$P(\theta, \phi) = \begin{bmatrix} \cos \theta \cos \phi \\ \cos \theta \sin \phi \\ \sin \theta \end{bmatrix} \quad (4)$$

Using Eq (2), we have obtained the Cartesian components of the electric field and reconstructed the local radial, azimuthal and longitudinal components of the complex electric field through the following transformations [1]:

$$\begin{aligned} E_r(\vec{r}, z) &= E_x(\vec{r}, z) \cos \phi_s + E_y(\vec{r}, z) \sin \phi_s \\ E_{\phi_s}(\vec{r}, z) &= E_y(\vec{r}, z) \cos \phi_s - E_x(\vec{r}, z) \sin \phi_s \\ E_z(\vec{r}, z) &= E_z(\vec{r}, z) \end{aligned} \quad (5)$$

The resultant electric field and its intensity in the focal region are given as:

$$\vec{E}(\vec{r}, z) = E_r(\vec{r}, z) \hat{e}_r + E_{\phi}(\vec{r}, z) \hat{e}_{\phi} + E_z(\vec{r}, z) \hat{e}_z \quad (6)$$

$$|E(\vec{r}, z)|^2 = |E_r(\vec{r}, z)|^2 + |E_{\phi}(\vec{r}, z)|^2 + |E_z(\vec{r}, z)|^2 \quad (7)$$

where \hat{e}_r , \hat{e}_{ϕ} and \hat{e}_z are the unit vectors along the radial, azimuthal and longitudinal directions, respectively. In our numerical evaluation, spatial coordinates are in the units of wavelength of light. Constant A is determined in such a way that the truncated beam carries same optical power in the entrance pupil for all modes. Optical power of a truncated second order radially polarized (R-TEM₁₁) beam with $\beta = 2$ and $A = 1$ is considered as standard and is used for normalization for R-TEM₀₁ mode.

3 Results and discussion

After obtaining the complex amplitudes of tightly focused radially polarized beams of first and second orders respectively from Eq (1) and Eq (2), the total intensities of radial and longitudinal polarization components are investigated for a focusing system. Table 1 shows the full width at half maximum (FWHM) values of the focal spot obtained for free space ($n = 1.0$) with two values of NA for radial and circular polarizations, respectively and it can be seen that in presence of spherical aberration, the FWHM decreases with increasing Numerical Aperture (NA). Also, the secondary lobes for the circularly polarized TEM₁₁ (C-TEM₁₁) beam are very dominant but it reduces in presence of spherical aberration and these results show very intricate relation of truncation parameter, modes and spherical aberration and polarization on tightly focused structure. We compared our results with that of tight focusing of R-TEM₀₁ beams and they agree well for aberration-free cases with the values reported in literature [2,18-20] and results of first order radially polarized beam in presence of aberration with the values reported by Biss and Brown [26].

Table 1. FWHM of the focal spot in free-space ($n = 1$)

Beam Mode	Full Width at Half Maximum (FWHM) (λ^{-1})							
	Radial Polarization				Circular Polarization			
	R-TEM ₀₁ (for $\beta = 1.3$)		R-TEM ₁₁ (for $\beta = 2$)		C-TEM ₀₁ (for $\beta = 1.3$)		C-TEM ₁₁ (for $\beta = 2$)	
	$A_s = 0.0$	$A_s = 0.5$	$A_s = 0.0$	$A_s = 0.5$	$A_s = 0.0$	$A_s = 0.5$	$A_s = 0.0$	$A_s = 0.5$
NA = 0.8	1.352	1.972	0.782	0.954	0.69	0.80	0.52	0.63
NA = 1.0	0.560	0.826	0.440	0.484	0.58	0.69	0.57	0.56

3.1 Effect of spherical aberration

In this section, results of numerical evaluations obtained for tight focusing of R-TEM₁₁ beam for values of $\beta = 2.0$ and 1.3 in presence of spherical aberration with different strengths are reported. Figure 2(a) to Fig 2(i) show the structure of the R-TEM₁₁ beam at the tight focusing spot for NA = 1.2, $n = 1.33$ in terms of total intensity distribution and intensity of radial and longitudinal polarization components at the focal plane for values of spherical aberration $A_s = 0, 0.5$, and 1.5 ; when $\beta = 2$. It can be seen that for different degrees of aberration levels in Fig 2 the amplitude scale changes. When comparing the image figures in the present paper, note that the amplitude scale changes between plots have different degrees of aberration. Figure 2(a), Fig 2(b) and Fig 2(c) show that the tight focusing of R-TEM₁₁ beam produces sharp peak at the focal point and the longitudinal polarization component, $|E_z|^2$ dominates when there is no spherical aberration ($A_s = 0$) and in a similar way Fig 2(d), Fig 2(e) and Fig 2(f) show the results of the tight focusing when $A_s = 0.5$ and Fig 2(g), Fig 2(h) and Fig 2(i) show the results for $A_s = 1.5$, respectively. It is clear from these results that when the strength of the spherical aberration increases, the strength of the longitudinal polarization component $|E_z|^2$ reduces and $|E|^2$, $|E_r|^2$ and $|E_z|^2$ values spread over a significant region in the focal plane. It is also observed from Fig 2 that the strength of the longitudinal component ($|E_z|^2$) is high in comparison to the radial polarization component ($|E_r|^2$) at the focal point when spherical aberration (A_s) is 1.5 . But, $|E_r|^2$ gains strength in comparison to the $|E_z|^2$ component at the non-focal point regions and this makes a small dip in $|E|^2$ around the focal point as shown in Fig 2(g). In a similar way, the intensity distributions of $|E|^2$, $|E_r|^2$ and $|E_z|^2$ in the x-z plane are shown from Fig 3(a) to Fig 3(i) for various spherical aberration values $A_s = 0.0, 0.5$ and

1.5 respectively. It can be seen from Fig 3 that the maximum peak values of $|E|^2$ and $|E_z|^2$ lie at the focal point for $A_s = 0.0$ (Fig 3(a) to Fig 3(c)) and the maximum peak shifts away from focal points for $A_s = 0.5$ (Fig 3(d) to Fig 3(f)) and $A_s = 1.5$ (Fig 3(g) to Fig 3(i)), respectively.

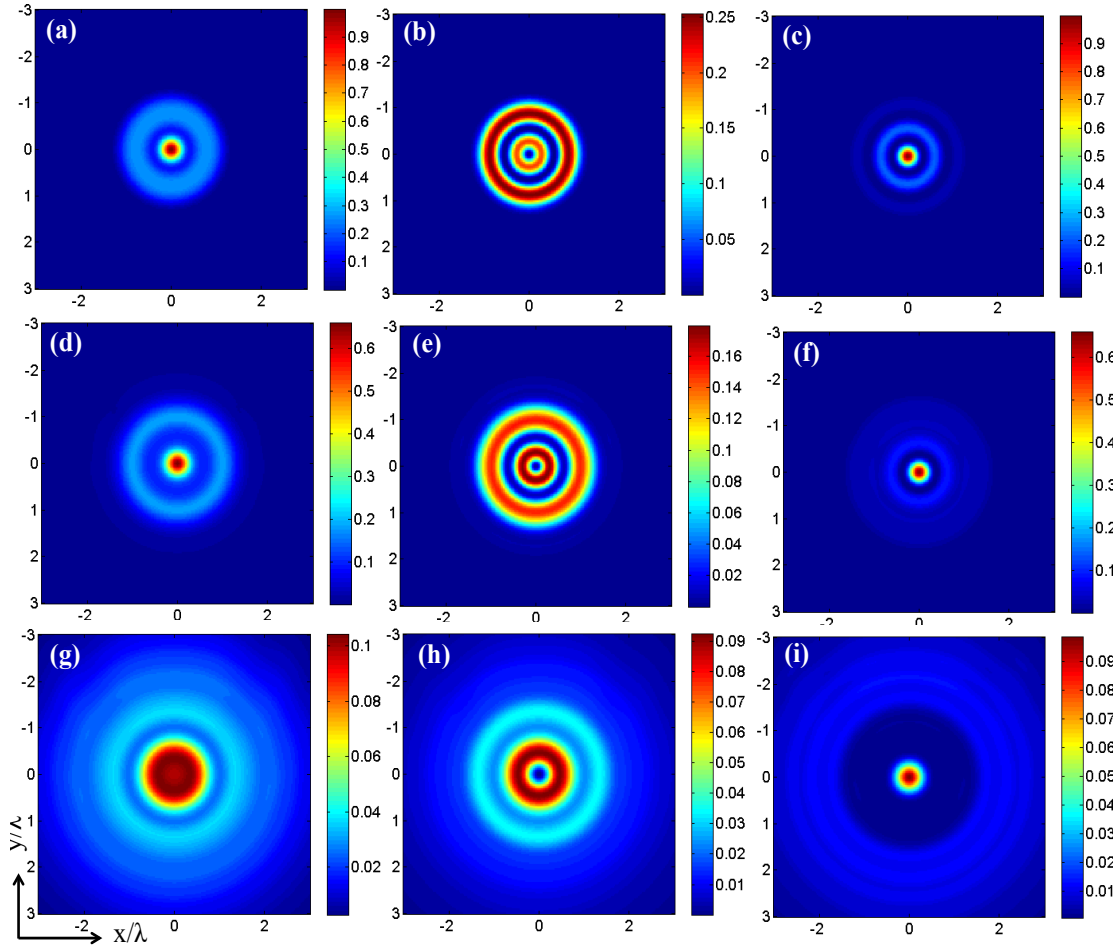


Fig 2. Structure of the R-TEM₁₁ beam with $\beta = 2$ at the focal spot for NA = 1.2, $n = 1.33$; $A_s = 0.0$ (a) $|E(r)|^2$ (b) $|E_r(r)|^2$ (c) $|E_z(r)|^2$; $A_s = 0.5$ (d) $|E(r)|^2$ (e) $|E_r(r)|^2$ (f) $|E_z(r)|^2$; $A_s = 1.5$ (g) $|E(r)|^2$ (h) $|E_r(r)|^2$ (i) $|E_z(r)|^2$

Similar analysis is also carried out for R-TEM₁₁ beam with $\beta = 1.3$ in presence and absence of spherical aberration (A_s). The results are shown from Fig 4(a) to Fig 4(i) for $A_s = 0.0, 0.5$ and 1.5 , respectively. It can be observed that zero intensity occurs at the focal point for $A_s = 0.0$ as shown from Fig 4(a) to Fig 4(c), which is in agreement with the results of Kozawa and Sato [18-20]. The peak intensities of $|E_r|^2$ and $|E_z|^2$ components are located at 0.64λ and 0.44λ from the focal spot as shown in Fig 4(b) and Fig 4(c), respectively. The ratio of peak strengths of the longitudinal and radial polarization components is 0.34 for $A_s = 0.0$. The intensity distributions of $|E|^2$, $|E_r|^2$ and $|E_z|^2$ at the focal plane of R-TEM₁₁ beam are shown in Fig 4 (Fig 4(d) to Fig 4(i)) when $\beta = 1.3$ for $A_s = 0.5$ and $A_s = 1.5$, respectively. The Figs 4(d) , 4(e) and 4(f) show that due

to presence of spherical aberration ($A_s = 0.5$), the null values of central intensity disappears and focal spot shrinks with restructuring of $|E_r|^2$ and $|E_z|^2$. For $A_s = 0.5$, $|E_r|^2$ component maintains zero at the focal point but primary ring shrinks and lies at 0.41λ . On the other hand, zero value of $|E_z|^2$ at the focal point is changed into the sharp peak and FWHM value of $|E_z|^2$ equals to 0.41λ for $A_s = 0.5$. The ratio of peak strengths of the longitudinal and radial polarization components becomes 1.85 for $A_s = 0.5$. Another observation is that in Fig 4(g), 4(h) and Fig 4(i) the strength of $|E_z|^2$ decreases with increase in the spherical aberration and the ratio of the peak strengths of longitudinal and radial polarization components becomes 0.34 for $A_s = 1.5$. The central dip shown in Fig 4(g) is due to high strength of $|E_r|^2$ around the focal point in comparison to $|E_z|^2$. The intensity distributions of $|E|^2$, $|E_r|^2$ and $|E_z|^2$ of R-TEM₁₁ beam in the x-z plane at focal point are shown in Fig 5 for different strengths of spherical aberration values ($A_s = 0.0, 0.5$ and 1.5) when $\beta = 1.3$.

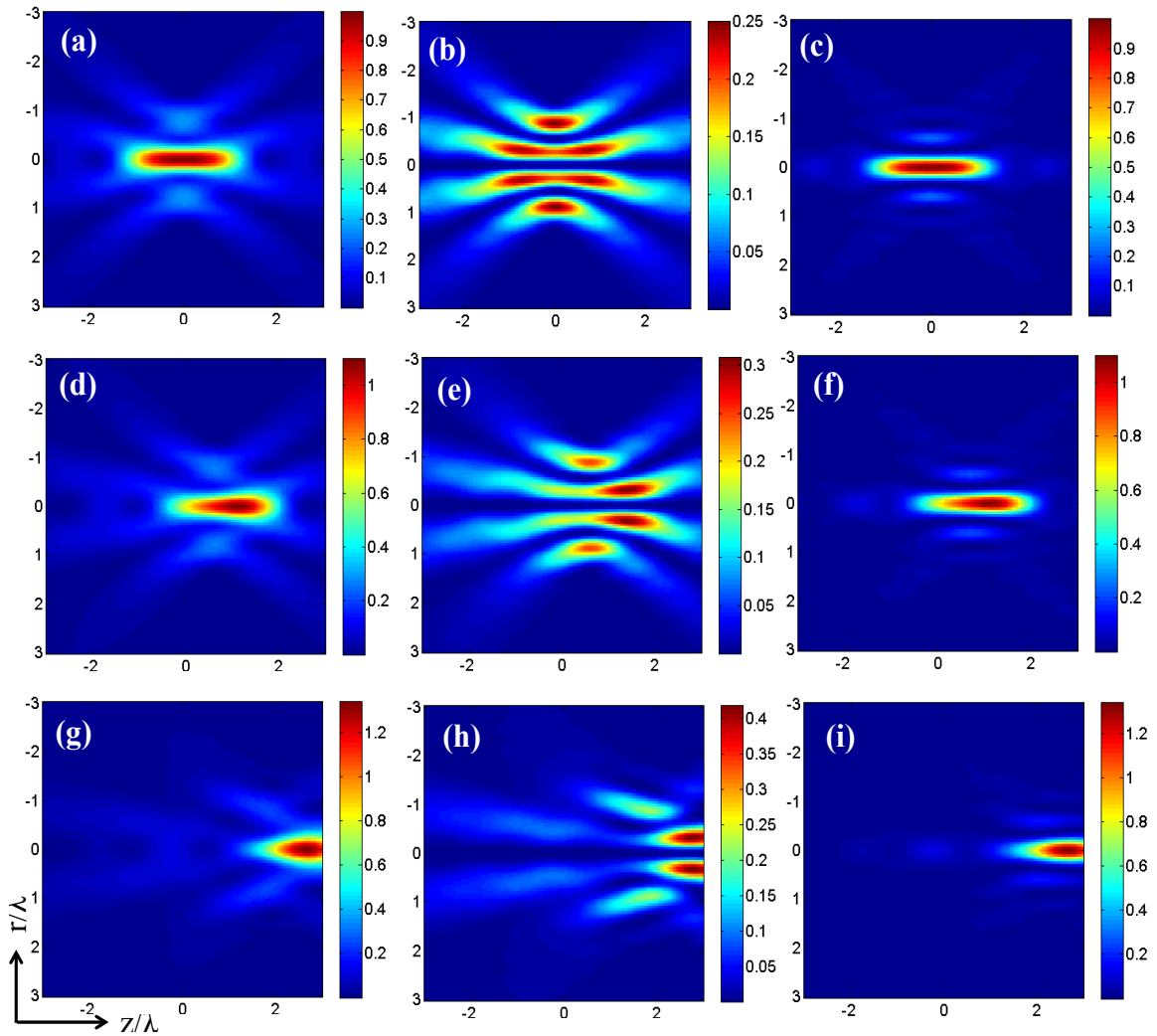


Fig 3. Structure of the R-TEM₁₁ beam at the focal spot in x-z plane with $\beta = 2$, $NA = 1.2$ and $n = 1.33$; $A_s = 0.0$ (a) $|E(r,z)|^2$ (b) $|E_r(r,z)|^2$ (c) $|E_z(r,z)|^2$; $A_s = 0.5$ (d) $|E(r,z)|^2$ (e) $|E_r(r,z)|^2$ (f) $|E_z(r,z)|^2$; $A_s = 1.5$ (g) $|E(r,z)|^2$ (h) $|E_r(r,z)|^2$ (i) $|E_z(r,z)|^2$

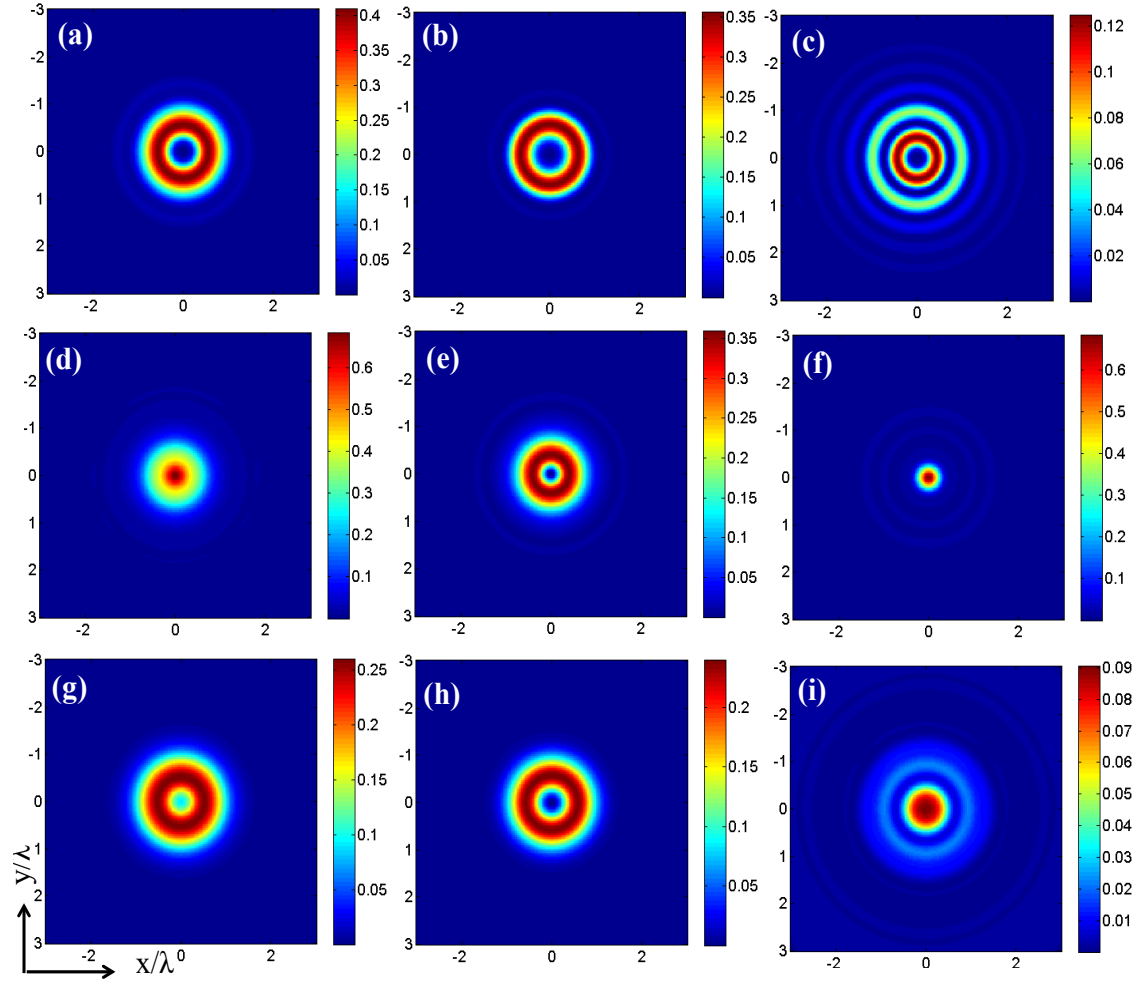


Fig 4. Structure of R-TEM₁₁ beam with $\beta = 1.3$ at the focal spot for NA = 1.2, $n = 1.33$; $A_s = 0.0$: (a) $|E(r)|^2$ (b) $|E_r(r)|^2$ (c) $|E_z(r)|^2$; $A_s = 0.5$: (d) $|E(r)|^2$ (e) $|E_r(r)|^2$ (f) $|E_z(r)|^2$; $A_s = 1.5$: (g) $|E(r)|^2$ (h) $|E_r(r)|^2$ (i) $|E_z(r)|^2$

The tight focusing of R-TEM₁₁ beam makes an optical cage like structure in aberration free case ($A_s = 0.0$) and this optical cage like structure disappears in presence of aberration ($A_s = 0.5$ and 1.5) due to shifting of the peak intensity from the focal plane and can be observed clearly from Fig 5(d) to Fig 5(f) for $A_s = 0.5$ and from Fig 5(g) to Fig 5(i) for $A_s = 1.5$, respectively. From these results (Fig 3 to Fig 5), it is observed that focal structure of the second order radially polarized beam is not only sensitive to truncation parameter β but also to the spherical aberration (A_s). Then, numerically we investigated the effect of truncation parameter, β at the tight focusing spot. The effect of the variation of truncation parameter (β) on the strength of the longitudinal polarization component at the focal point ($z = 0$), i.e., $|E_z(0)|^2$, for R-TEM₀₁ and R-TEM₁₁ beams is investigated at the focusing and defocusing planes in presence of spherical aberration value $A_s = 0.5$. The evaluations are carried out by varying β values in the range between $0 < \beta < 2.0$ and the results are shown in Fig 6. The strength of the longitudinal component, $(|E_z(0)|^2)$ normalized by its peak value decreases with increasing values of β for aberration free case ($A_s = 0.0$) as shown in the plot (a) of Fig 6(i). The overall

strength of the longitudinal component, $(|E_z(0)|^2)$ of R-TEM₀₁ beam decreases with increasing presence of the spherical aberration (plots (b) and (c) of Fig 6(i)), except in the central range of β values. In Fig 6(i), the plot (b) shows the compensation of the effect of spherical aberration by the presence of defocusing effect ($A_d = -A_s/2$), whereas plot (c) in Fig 6(i) shows the variation of $(|E_z(0)|^2)$ with β in presence of only spherical aberration i.e. when the defocusing coefficient, $A_d = 0$. The influence of spherical aberration is significant in the central range of β values.

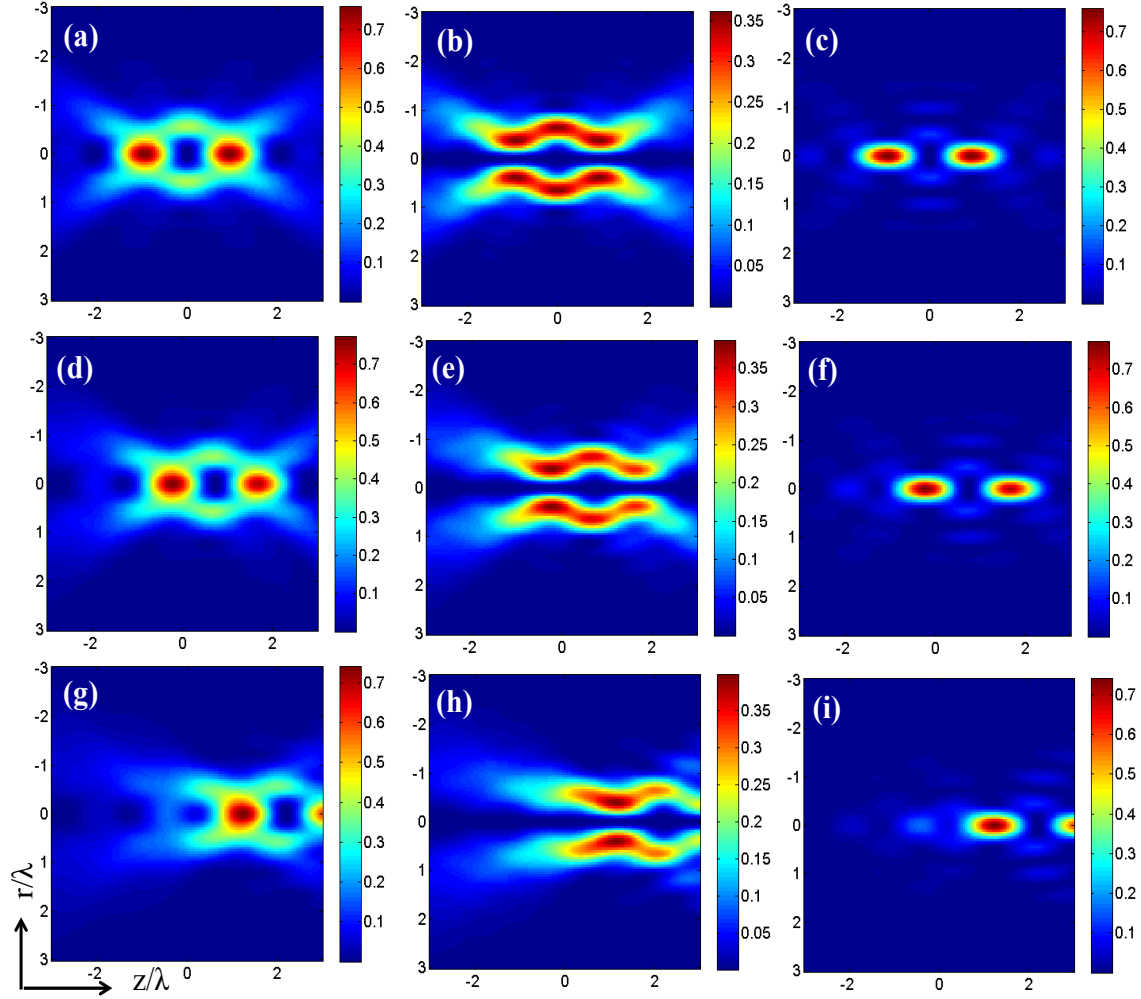


Fig 5. Structure of R-TEM₁₁ beam at the focal spot in x-z plane with $\beta = 1.3$, $NA = 1.2$ and $n = 1.33$; $A_s = 0.0$ (a) $|E(r,z)|^2$, (b) $|E_r(r,z)|^2$, (c) $|E_z(r,z)|^2$; $A_s = 0.5$ (d) $|E(r,z)|^2$, (e) $|E_r(r,z)|^2$, (f) $|E_z(r,z)|^2$; $A_s = 1.5$, (g) $|E(r,z)|^2$, (h) $|E_r(r,z)|^2$, (i) $|E_z(r,z)|^2$

The variation of the longitudinal component, $(|E_z(0)|^2)$ of R-TEM₁₁ beam with the variation of the truncation parameter, β is shown in Fig 6 (ii) in presence and absence of spherical aberration. It can be observed from the plot (a) of Fig 6(ii) that when $A_s = 0.0$, the intensity of the longitudinal component reduces with an increase in the truncation parameter and reaches to zero at $\beta = 1.3$ and the dip in the plot corresponds

to the formation of the optical cage like structure. Strengthening of $(|E_z(0)|^2)$ takes place in the range of $1.3 < \beta < 2.0$, but it starts reducing again when $\beta > 2.0$. Similarly, the variation of $(|E_z(0)|^2)$ with β for $A_s = 0.5$ and 1.5 is shown in plots (b) and (c) of Fig 6(ii). These results are similar to the plot (a) of Fig 6(ii) except for small deviation in the central region of β where intensity zero disappears. When the defocusing parameter is introduced ($A_d = -A_s/2$), the effect of the spherical aberration is compensated to some extent and is evident from the plot (b) of Fig 6(ii).

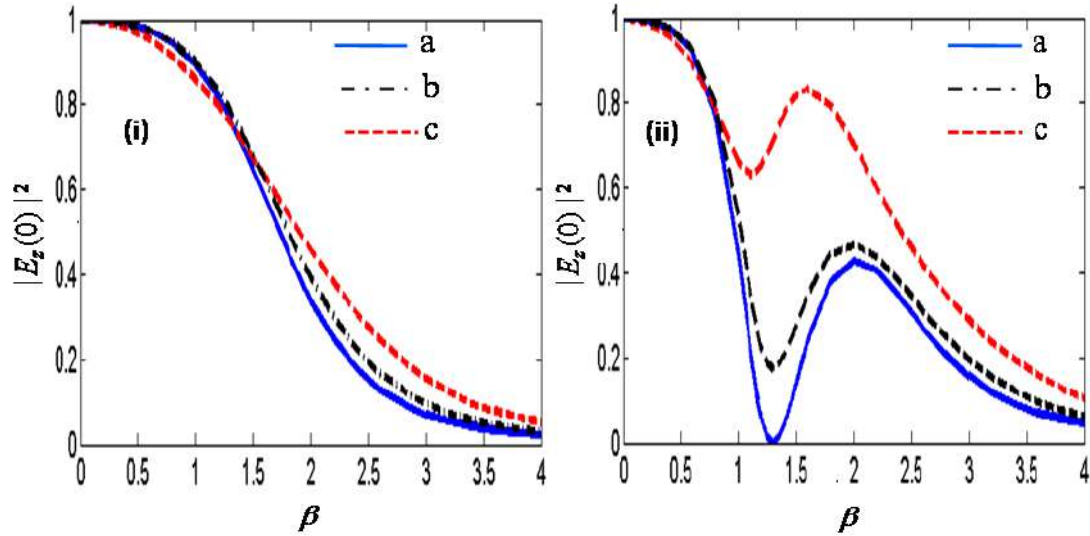


Fig 6. Variation of the longitudinal polarization component at the focal point $(|E_z(0)|^2)$ with the truncation parameter (β) for $NA = 1.2$, $n = 1.33$;

(i) R-TEM₀₁ and (a) $A_s = 0.0$, $A_d = 0.0$; (b) $A_s = 0.5$, $A_d = -A_s/2$; (c) $A_s = 1.5$, $A_d = 0.0$

(ii) R-TEM₁₁ and (a) $A_s = 0.0$, $A_d = 0.0$; (b) $A_s = 0.5$, $A_d = -A_s/2$; (c) $A_s = 1.5$, $A_d = 0.0$

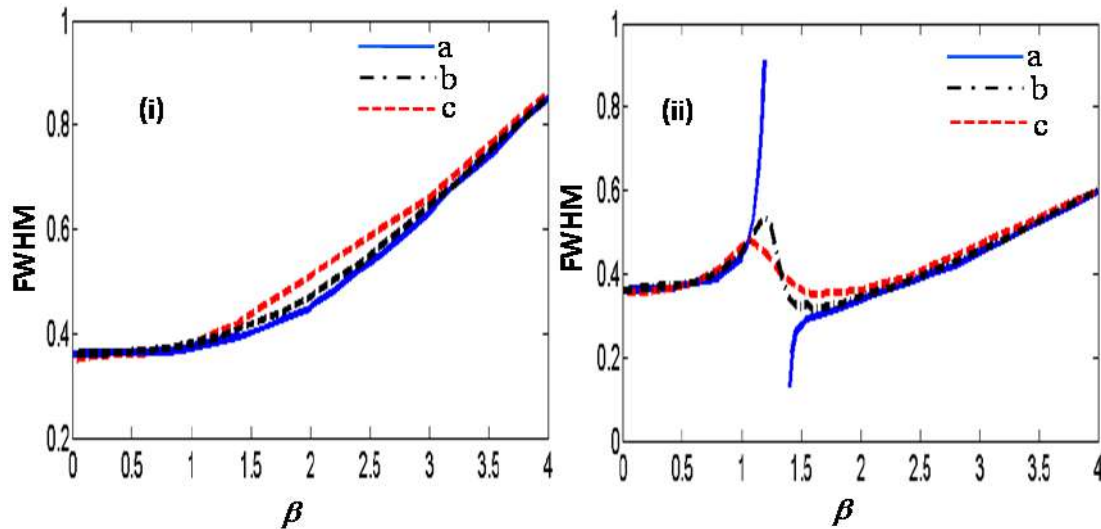


Fig 7. Variation of Full Width at Half Maximum (FWHM) of $|E_z|^2$ with β for $NA = 1.2$, $n = 1.33$. (i) R-TEM₀₁: (a) $A_s = 0.0$, $A_d = 0.0$; (b) $A_s = 0.5$, $A_d = -A_s/2$; (c) $A_s = 1.5$, $A_d = 0.0$; (ii) R-TEM₁₁: (a) $A_s = 0.0$, $A_d = 0.0$; (b) $A_s = 0.5$, $A_d = -A_s/2$; (c) $A_s = 1.5$, $A_d = 0.0$

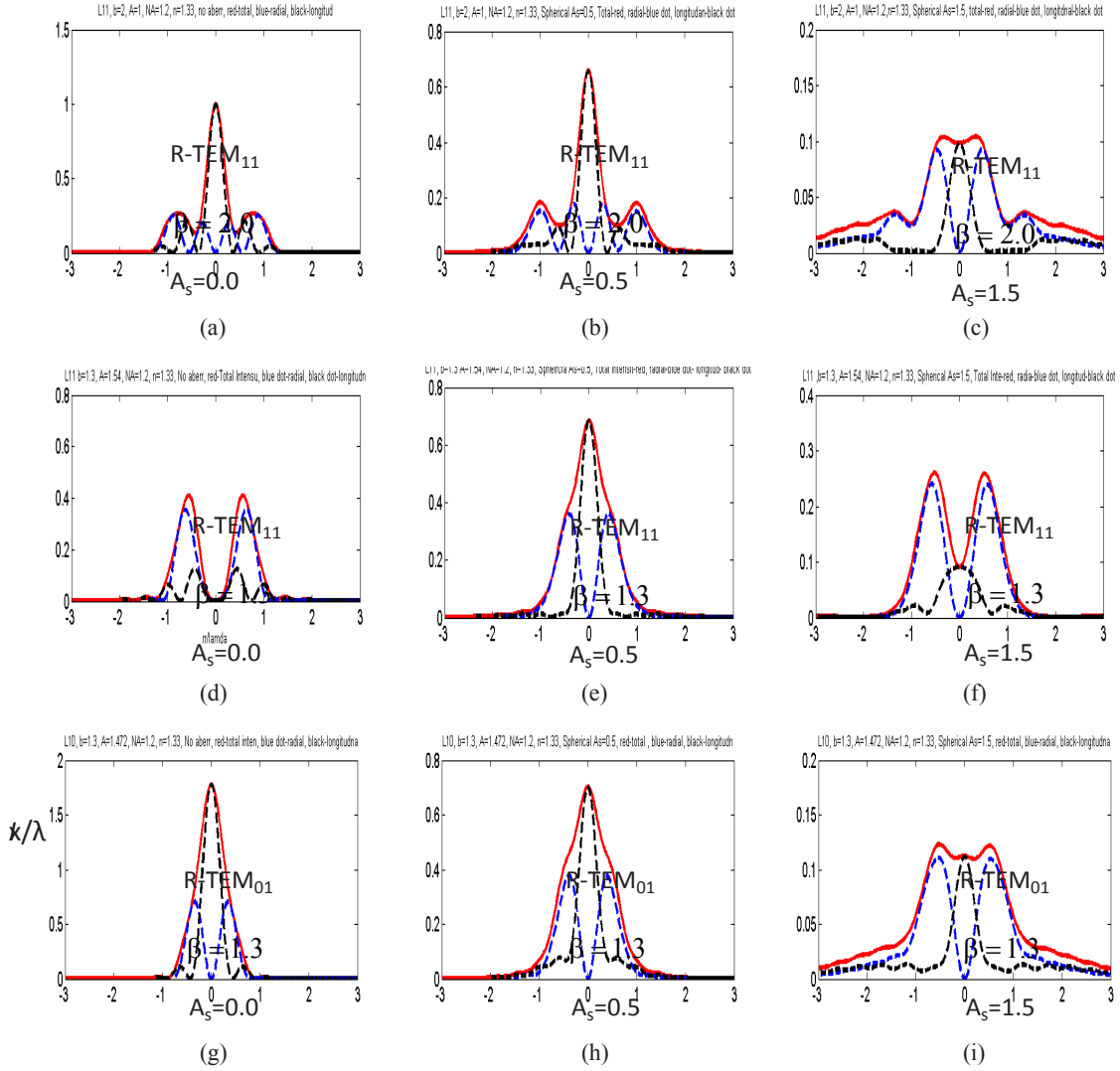


Fig 8. Profiles of the tightly focused radially polarized beams at $z = 0$ for $NA = 1.2$ and $n = 1.33$. Total intensity (red solid), longitudinal (black dotted) and radial polarization (blue dotted) components are drawn in each figure. R- TEM_{11} : (a) $A_s = 0.0$ (b) $A_s = 0.5$ (c) $A_s = 1.5$ for $\beta = 2.0$; R- TEM_{11} : (d) $A_s = 0.0$ (e) $A_s = 0.5$ (f) $A_s = 1.5$ for $\beta = 1.3$; R- TEM_{01} : (g) $A_s = 0.0$ (h) $A_s = 0.5$ (i) $A_s = 1.5$ for $\beta = 1.3$.

Another analysis carried out is the change in the focal spot of the intensity distribution of longitudinal polarization component, $(|E_z|^2)$ for different β values and for the R- TEM_{01} and R- TEM_{11} beams, respectively. The plots obtained are shown in Fig 7(i) and Fig 7(ii), respectively in which the full width half maxima (FWHM) values are measured to check change in the longitudinal polarization focal spot. The FWHM of the R- TEM_{01} beam increases with increasing truncation parameter β and is significant for the region $\beta > 1.4$ (shown in plot (a) of Fig 7(ii)). The influence of the spherical aberration on FWHM in presence ($A_d = -A_s/2$) and absence ($A_d = 0$) of defocusing is shown in the plots (b) and (c) of Fig 7(i), respectively. It can be observed from the plot (b) of Fig 7(i) that the defocusing ($A_d = -A_s/2$) compensates the effect of the

spherical aberration on FWHM. The variation of FWHM of R-TEM₁₁ beam with β is shown in Fig 7(ii) and is significantly different from the results of R-TEM₀₁ beam. The FWHM of R-TEM₁₁ beam when $A_d = 0$, is shown in the plot (a) of Fig 7(ii). The FWHM of R-TEM₁₁ beam is smaller than that of R-TEM₀₁ beam when $\beta > 2$. The influence of defocusing and spherical aberration on FWHM of the longitudinal component is shown in the plots (b) and (c) of Fig 7(ii). From Fig 7 it is also evident that the formation of optical cage like structure depends on the truncation parameter and strength of the spherical aberration (A_s).

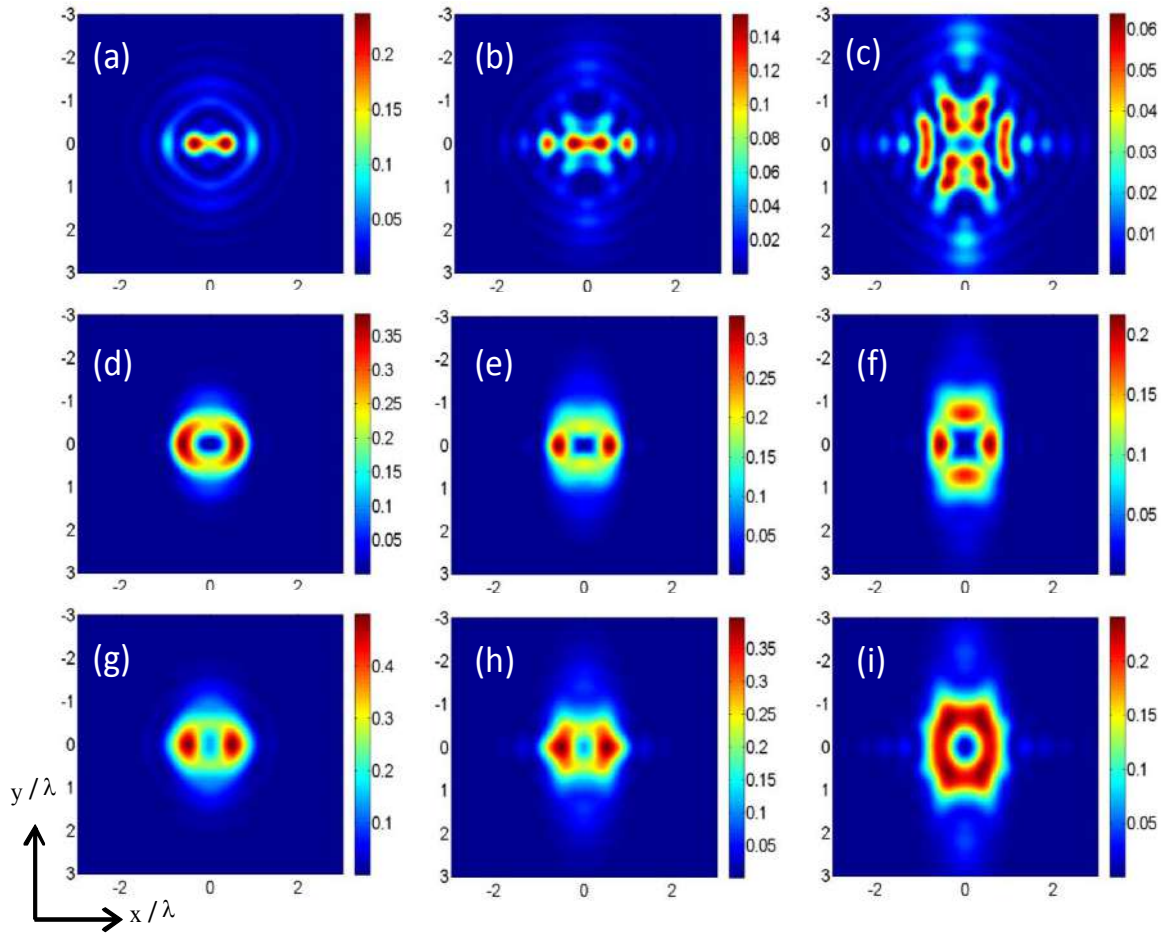


Fig 9. Structure of the R-TEM₁₁ beam with $\beta = 1.3$ at the focal plane for NA = 1.2, $n = 1.33$. Effect of astigmatism: on $|E_z(r)|^2$ (a) $A_a = 0.5$, (b) $A_a = 1$, (c) $A_a = 1.5$; on $|E_r(r)|^2$ (d) $A_a = 0.5$, (e) $A_a = 1$, (f) $A_a = 1.5$; on $|E|^2$ (g) $A_a = 0.5$, (h) $A_a = 1$, (i) $A_a = 1.5$.

The profiles of the total intensity and intensity of the radial and longitudinal components of the tightly focused R-TEM₀₁ and R-TEM₁₁ beams at $z = 0$ for NA = 1.2 and $n = 1.33$ at the focal point are plotted in Fig 8. The results are normalized by the peak intensity of R-TEM₁₁ mode when $\beta = 2.0$ for aberration free case ($A_s = 0$). Figures from 8(a) to 8(c) are plotted for R-TEM₁₁ beam with $\beta = 2.0$ when $A_s = 0.0, 0.5$ and 1.5, respectively. Figure 8(a) shows that $|E_z|^2$ dominates in shaping the focal structure of the beam, when there is no spherical aberration ($A_s = 0$). The spherical aberration values affect the longitudinal component, $|E_z|^2$ as shown from Fig 8(b) and Fig 8(c) for $A_s = 0.5$ and 1.5, respectively. The value of $|E_z|^2$ reduces for $A_s = 1.5$ and the peak value of radial component $|E_r|^2$ is nearly same as that of the longitudinal component ($|E_z|^2$).

The results obtained for R-TEM₁₁ beam with $\beta = 1.3$ are shown from Fig 8(d) to Fig 8(f). It is observed from Fig 8 that the focusing of R-TEM₁₁ beam with $\beta = 1.3$ forms an optical cage like structure in the absence of aberration. In this case, $|E_z|^2$ component is weak at non-focal points in comparison to the $|E_r|^2$ component but $|E_z|^2$ gains its strength at the focal point when $A_s = 0.5$ and this results in deformation of the optical cage like structure as shown in Fig 8(e). Again, $|E_z|^2$ loses its dominance in focal shaping for $A_s = 1.5$, and a dip appears in the total intensity plot. Therefore, existence of the optical cage like structure is highly susceptible to both spherical aberration and truncation parameter values of the second order radially polarized beam. Figure 8(g), Fig 8(h) and Fig 8(i) show the profiles of R-TEM₀₁ beam and the FWHM of $|E_z|^2$ for R-TEM₀₁ beam is 0.39λ in contrast to 0.56λ of R-TEM₁₁ beam when there is no spherical aberration ($A_s = 0$). The FWHM values of total intensity, $|E|^2$ for R-TEM₀₁ and R-TEM₁₁ beams are 0.64λ and 0.67λ , respectively. When spherical aberration is introduced with $A_s = 0.5$ and 1.5 , respectively then, spreading of the focal spot occurs with a reduction in the peak value of the longitudinal component. At the same time, the strength of the radial component increases in presence of spherical aberration and becomes prominent whenever $A_s = 1.5$ (Fig 8(i)).

3.3 Effects of astigmatism and coma

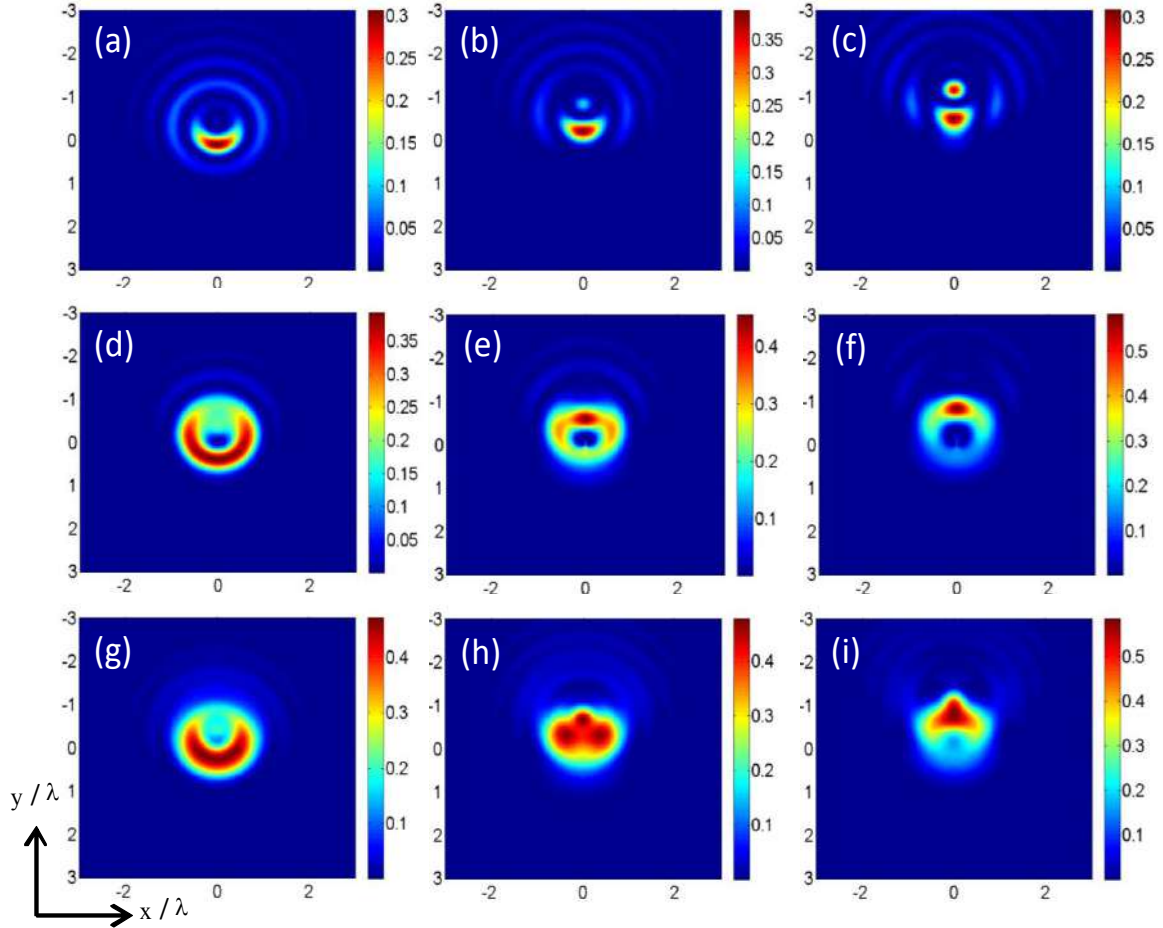


Fig 10. Effect of coma on the structure of R-TEM₁₁ beam with $\beta = 1.3$ at the focal plane for $NA = 1.2$, $n = 1.33$. $|E_z(r)|^2$: (a) $A_a = 0.5$, (b) $A_a = 1$, (c) $A_a = 1.5$; $|E_r(r)|^2$: (d) $A_a = 0.5$, (e) $A_a = 1$, (f) $A_a = 1.5$; on $|E|^2$ (g) $A_a = 0.5$, (h) $A_a = 1$, (i) $A_a = 1.5$.

In this section, we investigated the effect of astigmatism and coma on the tight focusing of R-TEM₁₁ beams for NA = 1.2, $n = 1.33$ and $\beta = 1.3$, where we observed the optical cage like structure. **Figures** from 9(a) to 9(c) show the longitudinal component value i.e $|E_z|^2$, **Figs** from 9(d) to 9(f) show the radial component value i.e $|E_r|^2$ and **Figs** from 9(g) to 9(i) show the total intensity in the transverse plane of the focused R-TEM₁₁ beam for varying values of astigmatism, $A_a = 0.5, 1$ and 1.5 , respectively. It can be observed from **Fig 9** that the astigmatism introduces asymmetry in the optical cage like structure and the asymmetry increases with increase in the strength of the astigmatism. The asymmetry can be explained due to the fact that vertically polarized tangential ray fan and horizontally polarized sagittal ray fan have different foci which can also introduce a phase shift between the two ray fans [26]. **Figures** from 10(a) to 10(c) show the longitudinal component, $|E_z|^2$, **Figs** from 10(d) to 10(f) show the radial component, $|E_r|^2$ and **Figs** from 10(g) to 10(i) show the total intensity in the transverse plane of the focused R-TEM₁₁ beam for varying values of coma, $A_c = 0.5, 1$ and 1.5 , respectively. It can be observed from **Fig 10** that coma destroys the rotational symmetry of the optical cage like structure and the rotational asymmetry increases with increase in the strength of the coma.

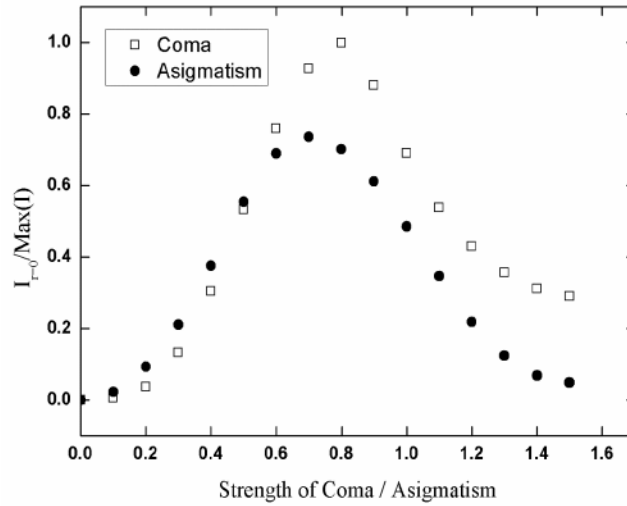


Fig 11. Normalized intensity at the centre of the optical cage structure as a function of the strength of coma (open squares) and astigmatism (solid circle).

To see more clearly the effects of astigmatism and coma on the intensity variations of the focal spot especially on the optical cage structure, we have calculated the ratio between the maximum intensity of the focal spot and the intensity at the centre of the optical cage like structure for different strengths of astigmatism and coma and the results are shown in **Fig 11**. It is clearly seen from **Fig 11** that the variation of the intensity ratio is asymmetric in case of coma in comparison with astigmatism. The intensity ratio is high for coma than astigmatism and it shows that the intensity at the centre of the optical cage structure increases with increase in the strength of coma due to increase in the rotational asymmetry and also size of the focal spot. It can also be observed that the intensity ratio gets highest value more quickly in case of astigmatism than coma due to rapid variation in the foci of tangential ray fan and sagittal ray fan.

4 Conclusion

We have investigated the effect of primary aberrations on tight focusing of second order radially polarized beams. The intensity distributions near the focal point for second order radially polarized beam

with spherical aberration are discussed for different truncation parameters. The results are compared with those of first order radially polarized beam. It is demonstrated that focal structure of the second order radially polarized beam is susceptible to both spherical aberration and truncation parameter values. It is also shown that the symmetry of the optical cage like structure in the focal plane depends on strength of astigmatism and coma.

Acknowledgment

MMB thanks IIT Kharagpur and DST for financial support. One of the authors (RKS) acknowledges IIST's fast track project support scheme.

References

1. Youngworth K S, Brown T G, *Opt Exp*, 7(2000)77-.
2. Quabis S, Dorn R, Eberler M, Glocke O, Leuchs G, *Opt Commun*, 179(2000)1.
3. Zhan Q, Leger J R, *Opt Express*, 10(2002)324-331.
4. Dorn R, Quabis S, Leuchs G, *Phys Rev Lett*, 91(2003)233901; doi.org/10.1103/PhysRevLett.91.233901
5. Sheppard C J R, Choudhury A, *Appl Opt*, 43(2004)4322-4327.
6. Sheppard C J R, Rehman S, Balla N K, Yew E Y S, Teng T W, *Opt Commun*, 282(2009)4647-4656.
7. Boruah B R, *J Opt Soc Am A*, 29(2012)1269-1276.
8. Chen Z, Hua L, Pu J, Tight focusing of light beams: Effect of polarization, phase and coherence, (ed. Wolf E), *Progress in Optics*, 57(2012)219-253.
9. Khoina S N, Golub I, *J Opt Soc Am A*, 30(2013)2029-2033.
10. Zhan Q, *Opt Lett*, 31(2006)1726-1728
11. Zhan Q, *Opt Express*, 12(2004)3377-3382.
12. Niziev V G, Nesterov A V, *J Phy D*, 32(1999)1455; doi.org/10.1088/0022-3727/32/13/304
13. Lan T H, Tien C H, *J Appl Phys*, 46(2007)3758-3760.
14. Tidwell S C, Kim G H, Kimura W D, *Appl Opt*, 32(1993)5222-5229.
15. Moser T, Glur H, Romano V, Pigeon F, Parriaux O, Ahmed M A, Graf T, *Appl Phys B*, 80(2005)707-713.
16. Kozawa Y, Sato S, *Opt Lett*, 30(2005)3063-3065.
17. Yonezawa K, Kozawa Y, Sato S, *Opt Lett*, 31(2006)2151-2153.
18. Kozawa Y, Sato S, *Opt Lett*, 31(2006)820-822.
19. Kozawa Y, Sato S, *J Opt Soc Am A*, 24(2007)1793-1798.
20. Kozawa Y, Sato S, *J Opt Soc Am A*, 29(2012)2439-2443.
21. Rajesh K B, Veerabagu Suresh N, Anbarasan P M, Gokulakrishnan K, Mahadevan G, *Opt Laser Technol*, 43(2011) 1037-1040
22. Guo H, Weng X, Jiang M, Zhao Y, Sui G, Hu Q, Wang Y, Zhuang S, *Opt Express*, 21(2013)5363-5372.
23. Kozawa Y, Hibi T, Sato A, Horanai H, Kurihara M, Hashimoto N, Yokoyama H, Nemoto T, Sato S, *Opt Express*, 19(2011)15947-15954.
24. Kant R, *J Mod Opt*, 40(1993)2293-2310.
25. Braat J J M, Dirksen P, Janssen A J E M, van de Nes A S, *J Opt Soc Am A*, 20(2003)2281-2292.
26. Biss D P, Brown T G, *Opt Express*, 12(2004)384-393.
27. Singh R K, Senthilkumaran P, Singh K, *J Opt Soc Am A*, 25(2008)1307-1318.
28. Singh R K, Senthilkumaran P, Singh K, *J Opt A: Pure Appl Opt*, 10(2008)075008; doi.org/10.1088/1464-4258/10/7/075008
29. Singh R K, Tight focusing of singular beams; Effect of primary aberrations, (LAP Lambert Academic Publishing), 2010.

30. Richards B, Wolf E, *Proc Roy Soc A*, 253(1959)358-379; doi.org/10.198/rspa.1959.0200
31. Torok P, Varga P, Laczik Z, Booker G R, *J Opt Sot Am A*, 12(1995)325-332.

[Received: 7.12.2015; accepted: 30.12.2015]

Maruthi Manoj Brundavanam

Dr. Maruthi Manoj Brundavanam obtained his Master degree in 2004 and Ph D in 2010 from the University of Hyderabad. He worked as a UEC Postdoctoral Fellow at the University of Electro-Communications, Tokyo, Japan till 2013. Later, he joined Department of Physics, Indian Institute of Technology Kharagpur in 2013 as Assistant Professor and still continuing. He is a member of the Optical Society of America (OSA) and life member of the Optical Society of India (OSI) and Indian Laser Association (ILA).



He was awarded Young Scientist Award by the KV Rao Scientific Society in 2009 and INSPIRE Faculty award by the DST-India in 2013. His research interests are in optical interferometry, optical beam shaping, singular optics and correlation optics.

Rakesh Kumar Singh

Dr. Rakesh Kumar Singh obtained his Master degree from the Banaras Hindu University and Ph D from the Indian Institute of Technology Delhi in 2009. He worked as postdoctoral researcher at the University of Oulu, Finland during January 2009 - July 2009, and later moved to the University of Electro-Communication, Tokyo as JSPS postdoctoral researcher and worked there till October 2011. Subsequently, he joined the Department of Physics, Indian Institute of Space Science and Technology (IIST), Trivandrum as Assistant Professor.



He is a member of the Optical Society of America, member of SPIE. His research interests are in the fundamental and applied optics and research works cover light shaping, singular optics, optical imaging, coherence optics, computational optics, laser speckles and polarization optic.